ACS Sustainable Chemistry & Engineering

Research Article

Cite This: ACS Sustainable Chem. Eng. 2018, 6, 3426−3433

pubs.acs.org/journal/ascecg

Free-Standing, Binder-Free Titania/Super-Aligned Carbon Nanotube Anodes for Flexible and Fast-Charging Li-Ion Batteries

Kunlei Zhu,[†] Yufeng Luo,[‡] Fei Zhao,[‡] Jiwei Hou,[†] Xuewen Wang,[†] He Ma,[§] Hui Wu,[†] Yuegang Zhang,[‡] Kaili Jiang,[‡] Shoushan Fan,[‡] Jiaping Wang,*[,‡] and Kai Liu*[,†]

[†]State Key Laboratory of New Ceramics and Fine Processing, School of Materials Science and Engineering, Tsinghua University, Beijing 100084, People's Republic of China

[‡]Department of Physics and Tsinghua-Foxconn Nanotechnology Research Center, Tsinghua University, Beijing 100084, People's Republic of China

[§]College of Applied Sciences, Beijing University of Technology, Beijing 100124, People's Republic of China

Supporting Information

ABSTRACT: Flexible and durable electrode materials are of vital importance to developing advanced energy storage devices for emerging wearable electronics. Most current strategies adopt chemical modifications or chemical binders to improve the interface interaction between flexible components, which inevitably lowers the cyclic lifetime and increases the production cost. Here, we report an in situ, scalable sol−gel method to fabricate free-standing TiO_2/superaligned carbon nanotube (SACNT) hybrid films as flexible anodes in Li-ion batteries. The natural and desirable wettability between TiO_2 and SACNTs makes any chemical modifications or chemical binders unnecessary in the fabrication process, delivering a clean TiO_2−SACNT interface. The as-prepared TiO_2/SACNT anodes not only inherit the high flexibility of the SACNT framework but also enhance rate capability and charge/discharge reversibility with its pseudocapacitive storage mechanism. These anodes exhibit a high capability and a long cyclic lifetime (over 1000 cycles at 60 C) in half cells. They are further assembled to make flexible full cells, where binders, conductive agents, and current collectors are all unnecessary. The capacity decay of a full-cell test is almost negligible over 500 cycles of bending with a fast charging rate within 50 s, suggesting TiO_2/SACNT films to be a promising material for flexible storage devices.

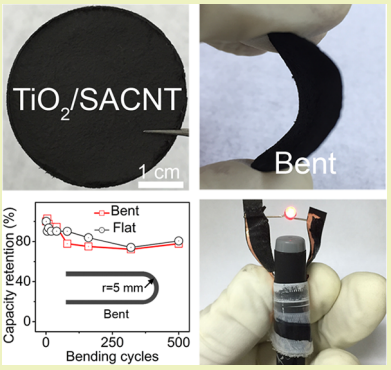

KEYWORDS: *Flexible Li-ion batteries, sol−gel, free-standing, TiO_2, carbon nanotube*

INTRODUCTION

In recent years, flexible electronic components have been intensively investigated to meet the increasing demands of wearable electronics.[1−4] It follows naturally that the development of flexible energy storage devices (e.g., flexible batteries and supercapacitors) are necessary to power these wearable electronics.[5,6] Owing to their high energy density, long lifetime, and high operation voltage, flexible Li-ion batteries attract widespread attention.[7−11] The fabrication and design of free-standing electrodes are crucial for these flexible batteries.[12,13] In this regard, carbon nanotube (CNT)-based hybrid films, because of their extremely flexibility, good electrical conductivity, and high mechanical strength, have been proved to be a promising candidate for flexible electrodes.[6] So far, the CNT-based anodes developed include CNT-cellulose-RTIL nanocomposite sheets;[14] free-standing single-walled CNT/SnO_2 anode paper;[15] and CNT-supported TiO_2, $Li_4Ti_5O_{12}$, $LiFePO_4$, and $LiCoO_2$ electrodes.[16−19] The sol−gel method is one of the most commonly used for preparations of CNT-based hybrids (e.g., SnO_2/CNT and Co_3O_4−SnO_2/CNT).[20] However, CNTs have to be modified by strong oxidizing acids[20−23] or surfactants[15,20,24] to improve the interface interaction for the homogeneous coating of these materials, which lowers the conductivity and strength of hybrid films as well as their performance as anodes. Therefore, delicate selection of active materials that have naturally good wettability with CNTs is much desired to avoid the usage of any chemical modifications or chemical binders.

TiO_2 has been reported to disperse on CNTs uniformly,[25] which may be caused by the strong interaction between CNTs and Ti with unfilled 3d orbitals as implied by the good wettability of Ti metal on CNTs.[26] Theoretical study shows that TiO_2 and CNTs can be bound through physical adsorption with a Ti−C noncovalently bonded interaction.[27,28] TiO_2 is also one of the most promising anode materials for Li-ion batteries,[29−33] because it exhibits small lattice change (<4%) during lithium insertion/extraction and a high operating voltage of 1−3 V (vs Li^+/Li). Due to these merits, TiO_2 can avoid the collapse of electrodes and suppress the formation of solid electrolyte interface (SEI) layers and lithium dendrites that

Received: October 10, 2017
Revised: December 8, 2017
Published: January 9, 2018

DOI: 10.1021/acssuschemeng.7b03671
ACS Sustainable Chem. Eng. 2018, 6, 3426−3433

could appear in the traditional carbon anodes, providing Li-ion batteries with better stability and safety. Its low cost, good availability, and environmental friendliness are very favorable for the massive manufacture of anodes of Li-ion batteries.

In this article, we report an *in situ*, scalable sol−gel method to fabricate free-standing TiO_2/SACNT hybrid films as flexible anodes in Li-ion batteries. The natural and desirable wettability between TiO_2 and SACNT delivers a clean interface between TiO_2 and SACNTs. The as-prepared TiO_2/SACNT anodes not only inherit the high flexibility of the SACNT framework but also enhance energy capability and charge/discharge reversibility with its pseudocapacitive storage mechanism. The flexible TiO_2/SACNT films provide a discharge capacity of ∼100 mA h g^{-1} at 60 C (1 C = 170 mA g^{-1}) over 1000 cycles when tested as an anode on half cells. They are further assembled to make flexible full cells, where binders, conductive agents, and current collectors are all unnecessary. The capacity decay is almost negligible in full-cell tests for over 500 cycles of bending with a fast charging rate within 50 s, which proves the TiO_2/SACNT films are a promising material for flexible storage devices.

EXPERIMENTAL SECTION

Materials. Tetrabutyl titanate (TBT, ≥99.7%) and concentrated ammonia−water (28%−30%) were purchased from Sigma-Aldrich. Anhydrous ethanol (≥99.5%) was obtained from Aladdin (Shanghai, China). $LiMn_2O_4$ (LMO) particles (10 μm) were purchased from Reshine in China. The superaligned CNT (SACNT) arrays with a diameter of 20−30 nm were fabricated on silicon wafers in a low pressure chemical vapor deposition system by using iron as the catalyst and acetylene as the precursor. The details of the preparation process can be found elsewhere.[34−36]

Methods. Free-standing flexible TiO_2/SACNT films were prepared using a facile *in situ* sol−gel method. In a typical synthesis, 40 mg SACNT arrays were scraped off the Si wafer and dispersed in 200 mL of ethanol using an intensive ultrasonication probe (SCIENTZ-950E, Ningbo, China) for 1 h to form SACNT dispersion solution. Then, 0.6 mL of concentrated ammonia−water was added to the above SACNT dispersion solution. After stirring for 10 min at 25 °C, 2 mL of TBT was dropwise added into the above dispersion solution. The reaction mixture was kept at 25 °C with continuous stirring for 8 h. Next, the mixture dispersion solution was filtered by vacuum filtration, and a flexible continuous TiO_2/SACNT film was formed on the filter paper. Finally, the free-standing flexible TiO_2/SACNT films (∼280 μm in thickness and ∼4 cm in diameter) were obtained after being dried in the air at room temperature. The amount of TiO_2 anchored on SACNTs can be enhanced by simply increasing the volume of concentrated ammonia−water (e.g 1.0 and 1.4 mL). For comparison, the scraped SACNT arrays were replaced by the commercial CNTs, and other conditions were kept unchanged. The free-standing LMO/SACNT films were prepared by a mixture of commercial LMO particles and the scraped SACNT arrays put into ethanol using ultrasonication, followed by a vacuum filtration.

To prepare TiO_2/SACNT films with high weight ratio TiO_2, we developed an improved sol−gel method. In a typical synthesis, 80 mg of SACNT arrays were scraped off the Si wafer and dispersed in 200 mL of ethanol using an intensive ultrasonication probe for 1 h to form SACNT dispersion solution in a beaker. Then, 2 mL of TBT was dropwise added into the above dispersion solution. The reaction mixture was kept at 25 °C with continuous stirring for 0.5 h. Next, the mixture dispersion solution was kept static at room temperature for 5−6 days in a fume hood until ethanol was completely volatile. TBT hydrolyzed with water in air slowly and continuously, and ultimately TiO_2 relatively covered the surface of SACNTs. Finally, the free-standing flexible TiO_2/SACNT films (Figure 4a) were obtained after being peeled off from the bottom of the beaker.

Characterizations and Measurements. Scanning electron microscopy (SEM) images were captured on a FEI Sirion 200 microscope (USA, 5 kV). Transmission electron microscopy (TEM) images, energy-dispersive X-ray (EDX) spectroscopy, high-angle annular dark-field scanning transmission electron microscopy (HAADF-STEM), and EDX elemental mapping images were collected with a FEI Tecnai G2F20 microscope (USA, 200 kV). X-ray diffraction (XRD) patterns were obtained on a Rigaku D/max 2500 PC diffractometer (Japan, 40 kV, 40 mA). X-ray photoelectron spectroscopy (XPS) experiments were conducted on a Thermal Fisher ESCALAB 250Xi spectrometer. For the *ex situ* XPS measurement, the discharged TiO_2/SACNT film was removed from the cell, washed with diethyl carbonate, and dried overnight in a glovebox (M. Braun inert gas system Co. Ltd., Germany) filled with high-purity argon. The film was sealed and rapidly transferred into the XPS chamber for measurement. Thermogravimetric (TGA) experiments were operated on a Netzsch STA449C instrument (Germany) from 25 to 800 °C under air with a heating rate of 10 °C min^{-1}.

Coin-type cells (2016 size) were assembled in the glovebox. The TiO_2 mass loading of TiO_2/SACNT films for each electrode is ∼1.3 mg cm^{-2}. For half cells, TiO_2/SACNT (LMO/SACNT) films were work electrodes, and pure lithium foils were both the counter and reference electrode with a cutoff voltage of 1.0−3.0 V (3.0−4.2 V). The specific capacities of the TiO_2/SACNT (LMO/SACNT) films are calculated based on the mass of TiO_2 (LMO). As for the coin-type and flexible full cells, free-standing TiO_2/SACNT films were used as anodes and free-standing LMO/SACNT films as cathodes with a cutoff voltage of 1.25−3.0 V. For full cells, the capacities of TiO_2/SACNT films are designed to be less than those of LMO/SACNT films, i.e., the TiO_2/SACNT-limited full cells. A porous polymer film (Celgard 2400, USA) was used as separator, and 1 M $LiPF_6$ was dissolved in a mixture of ethylene carbonate (EC), diethyl carbonate (DEC), and dimethyl carbonate (DMC) and used as an electrolyte (provided by Tianjin Jinniu Power Sources Material Co., Ltd). Galvanostatic charge/discharge tests were performed on a LAND CT2001A battery test system (Wuhan Land Electronic Co., China). Cyclic voltammetry (CV) curves (scan rate: 0.5−10 mV s^{-1}) and electrochemical impedance spectroscopy (EIS) tests (a perturbation of 5 mV applied) were operated on an EG&G Princeton Applied Research 273A potentiostat (Ametek, USA).

RESULTS AND DISCUSSION

Figure 1 provides a brief schematic illustration for the preparation of free-standing flexible TiO_2/CNT films. The

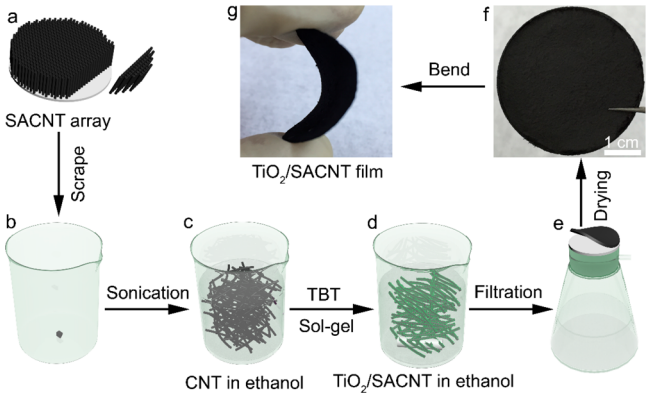

Figure 1. Schematic illustration of the preparation of the free-standing flexible TiO_2/CNT films.

superaligned CNT (SACNT) arrays were synthesized on SiO_2/Si wafers (Figure 1a) by chemical vapor deposition, as reported in our previous work.[34−36] The SACNT arrays were then scraped off (Figure 1b) and were dispersed in ethanol (Figure 1c) by ultrasonication, forming an expanded SACNT network in the SACNT-ethanol dispersion solution (Figure S1). TiO_2

DOI: 10.1021/acssuschemeng.7b03671
ACS Sustainable Chem. Eng. 2018, 6, 3426−3433

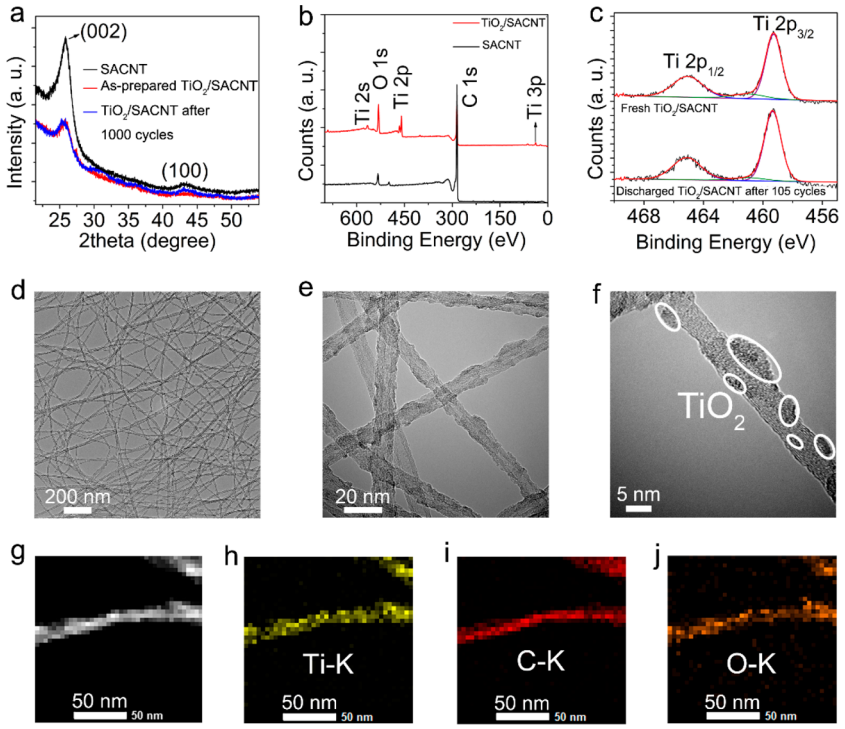

Figure 2. (a) XRD patterns, (b, c) XPS spectra, (d–f) TEM images, (g) HAADF-STEM image, and (h–j) EDX elemental mapping images of free-standing TiO_2/SACNT films.

nanoparticles were *in situ* formed on the dispersed SACNTs (Figure 1d) through hydrolysis and condensation of tetrabutyl titanate (TBT) in the SACNT-ethanol dispersion solution containing concentrated ammonia–water. Finally, TiO_2/SACNT films were obtained (Figure 1e) after vacuum filtration and air-drying. The TiO_2/SACNT films are free-standing (Figure 1f) and flexible (Figure 1g). The mass loading density of TiO_2 nanoparticles anchored on SACNT is estimated to be ~1.3 mg cm^{-2} by weighing the mass of TiO_2/SACNT films and subtracting the mass of SACNT based on the thermogravimetric (TGA) result. The weight ratio of TiO_2 is measured to be 28.7 wt % by TGA analysis, and this TiO_2/SACNT film is comprehensively discussed in the main text. The thickness and size of TiO_2/SACNT films can be regulated by the amount of TiO_2/SACNT solution and the diameter of the filtering flask, both of which could be easily scaled up. This facile process delivers continuous, highly flexible, and free-standing TiO_2/SACNT films, which benefits from the strong van der Waals interactions between the clean SACNTs derived from the high-quality SACNT arrays.[36] In comparison, we adopted commercial CNTs (C–CNT) to do similar experiments. The as-prepared TiO_2/C–CNT composites are found to be fragile and have difficulty forming continuous films (Figure S2).

The pristine SACNT and free-standing TiO_2/SACNT films were studied using X-ray diffraction (XRD) measurements in Figure 2a. The pristine SACNT film exhibits two peaks at 2θ = ~25.8° and 43° indexed to be the (002) and (100) reflections of SACNTs (Figure 2a, black line). For free-standing TiO_2/SACNT films (Figure 2a, red line), no XRD peaks of crystalline TiO_2 are observed, suggesting an amorphous structure of TiO_2 on SACNTs. To further verify their components, X-ray photoelectron spectroscopy (XPS) spectra were performed. After TiO_2 decorating, the peaks of Ti elements appear prominently in the spectrum of TiO_2/SACNT films (Figure 2b). The high-resolution XPS spectrum of the TiO_2/SACNT films in Figure 2c shows two peaks at 459.4 and 465.2 eV which are attributed to Ti $2p_{2/3}$ and Ti $2p_{1/2}$, respectively. The two Ti 2p peaks are highly symmetrical, without the shoulder peak at 456.9 eV that is typically associated with Ti^{3+}.[37] Moreover, the Ti/O ratio of the TiO_2/SACNT films is 2 after the removal of O content in SACNTs using XPS quantitative analysis, confirming that the hydrolyzed product is indeed TiO_2. In addition, we randomly choose three points of the TiO_2/SACNT films for Raman measurement (Figure S3). There are no typical peaks of TiO_2 besides the D and G peaks of SACNTs, potentially due to the weak Raman signal of amorphous TiO_2 that is overwhelmed by the strong signal from SACNTs. However, the D and G peaks of SACNTs shift toward high frequency. This blue shift could be indicative of the strong interactions between amorphous TiO_2 and SACNT, applying a strain on SACNTs during the formation of TiO_2 nanoparticles. Scanning electron microscopy (SEM) and transmission electron microscopy (TEM) images (Figure 2d–f and Figure S4) of free-standing TiO_2/SACNT films show a uniform distribution of TiO_2 nanoparticles. The high-resolution TEM image (Figure 2f) clearly shows that TiO_2 nanoparticles with diameters ranging from 3 to 10 nm are anchored on the surface of SACNTs, which is different from the pristine SACNTs with rather smooth surfaces (Figure S5). The energy-dispersive X-ray (EDX) spectroscopy (Figure S6) analysis also confirms the existence of Ti, C, and O elements in TiO_2/SACNT films, without other element contaminants. As shown in Figure 2g–j and Figure S7, high-angle annular dark-field scanning transmission electron microscopy (HAADF-STEM) and EDX elemental mapping images indicate that the TiO_2 nanoparticles are homogeneously distributed on the surface of SACNTs. The uniform coating may be attributed to the clean surfaces of SACNTs, which facilitates the wetting of TBT and the growth of TiO_2 on their surfaces. Furthermore, the formation of partial or uniform TiO_2 coatings on SACNTs

DOI: 10.1021/acssuschemeng.7b03671
ACS Sustainable Chem. Eng. 2018, 6, 3426–3433

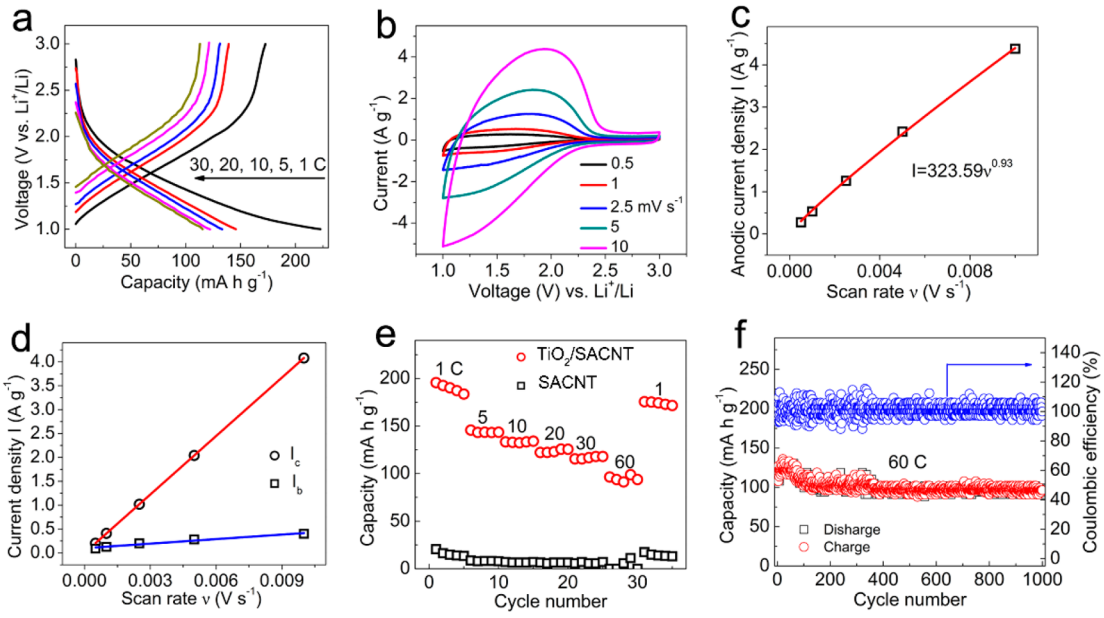

Figure 3. Electrochemical performance of the flexible TiO_2/SACNT films tested on half cells with the cutoff voltage of 1.0−3.0 V: (a) Galvanostatic charge/discharge curves, (b) CV curves, (c) scan rate (ν) vs anodic current (I) curve, (d) scan rate (ν) vs current (I_a and I_b) curve, (e) rate capacity curves, and (f) cycling and Coulombic efficiency curves at 60 C.

can be smoothly regulated by changing the amount of concentrated ammonia−water (Figure S8). And the mass ratio of TiO_2 varies from 28.7% to 46.3% to 60.8% given by TGA analysis in Figure S9.

We then turn to investigating the electrochemical performance of free-standing TiO_2/SACNT films assembled in half cells, with pure lithium foils as the counter and reference electrodes. Figure 3a shows the galvanostatic charge/discharge curves of TiO_2/SACNT films at various charge/discharge rates. The amorphous TiO_2/SACNT films show ambiguous plateaus with unclear contours, corresponding to the typically vague anodic and cationic peaks at ∼1.7 V and ∼1.5 V in the cyclic voltammetry (CV) curve (Figure S10a). This behavior is quite different from that of anatase TiO_2/SACNT films fabricated after the calcination at 400 °C in ambient air for 2 h (Figure S11a), which display distinct plateaus corresponding to the insertion/extraction of Li^+ ions (Figure S11b).[29,30] To clarify this abnormal behavior, CV curves of as-prepared amorphous TiO_2/SACNT films were reversibly measured at a 0.5−10 mV s^{-1} scan rate (Figure 3b and S10). The relationship between the current I and the sweep rates ν in the CV measurement follows the equation[38]

$$I = a\nu^b \tag{1}$$

where a and b are adjustable values. Typically, there are two well-defined values for b depending on the dominant mechanism. If b = 0.5, it shows that the Faradaic Li-insertion reaction involving a Li diffusion-controlled process dominates charge/discharge; if b = 1, on the other hand, a typical behavior of pseudocapacitive response would dominate.

The result in Figure 3c reveals that I is proportional to $\nu^{0.93}$ (the detailed analysis is available in Figure S12a), indicating that the Li storage could be attributed mostly to pseudocapacitive response and partially to Li insertion. We differentiate the contributions from pseudocapacitive behavior (I_c) and Li-insertion reaction (I_b; Figure 3c) using the reported method,[38,39] in which the current I can be expressed as

$$I = k_1\nu + k_2\nu^{1/2} \tag{2}$$

where $k_1\nu$ and $k_2\nu^{1/2}$ represent current contributions from I_c and I_b, respectively. The values of k_1 and k_2 are obtained by a linear fitting (available in Figure S12b). Figure 3d shows the values of $k_1\nu$ and $k_2\nu^{1/2}$, in which pseudocapacitive behavior dominates the current contribution at various sweep rates, especially at high sweep rates (Figure 3d). Therefore, the capacities of TiO_2/SACNT films mainly originate from the pseudocapacitive response involving a surface/interface Li storage process, not from a Li-insertion diffusion-controlled process. Furthermore, we conduct a cycling test of TiO_2/SACNT films for 105 cycles at 10 C to achieve stable capacities and keep it at the discharged state (Figure S13) to perform an *ex situ* XPS measurement. As shown in Figure 2c and Figure S14, the two Ti 2p peaks still remain at exactly the same positions as those of as-prepared TiO_2/SACNT film and are highly symmetrical with no shoulder peaks of Ti^{3+}, suggesting that there are no observable Li^+ ions inserted into TiO_2 nanoparticles. This further indicates that the storage of Li on the surface of TiO_2 nanoparticles is dominated by the pseudocapacitive effect. The free-standing TiO_2/SACNT films demonstrate impressive capacities of ∼190, ∼145, ∼135, ∼125, ∼120, and ∼100 mA h g^{-1} at 1, 5, 10, 20, 30, and 60 C, respectively, and the discharge capacity is still as high as ∼175 mA h g^{-1} when current density returns to 1 C (Figure 3e). And, SACNTs exhibit negligible capacities at various charge/discharge rates (e.g., < 8 mA h g^{-1} at 5 C and approaching 0 mA h g^{-1} at 60 C), suggesting that energy capacities of TiO_2/SACNT films mostly originate from TiO_2 nanoparticles. The cycling performance of TiO_2/SACNT films is shown in Figure 3f. After 1000 cycles at 60 C, they still have a capacity of ∼100 mA h g^{-1}, which is one of the best reported results under charge/discharge rates among TiO_2/C composites (Figure S15).[29−31,33,40−42,46] The Coulombic efficiency of each cycle approaches ∼100%. The structure of TiO_2/SACNT films remains unchanged after 1000 cycles at 60 C, as revealed by the

DOI: 10.1021/acssuschemeng.7b03671
ACS Sustainable Chem. Eng. 2018, 6, 3426−3433

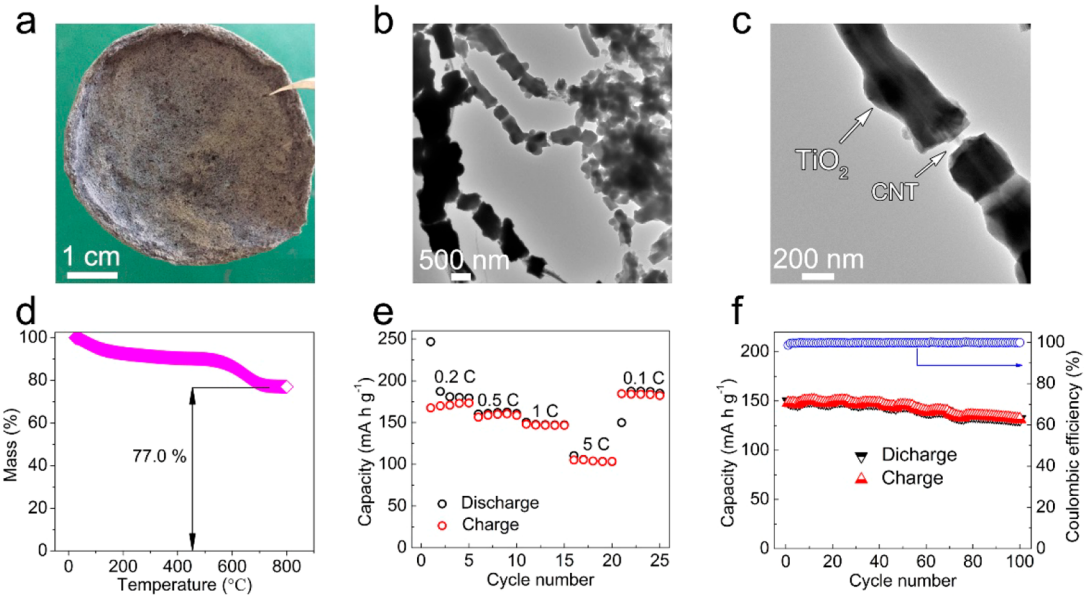

Figure 4. TiO_2/SACNT films with 77.0 wt % TiO_2: (a) a photograph, (b, c) TEM images, (d) TGA curve, (e) the rate capacity curves, and (f) cycle performance curve at 1 C. The capacities are estimated based on the mass of TiO_2/SACNT films.

XRD measurement (blue curve in Figure 2b) and the SEM image (Figure S16).

This excellent performance of free-standing TiO_2/SACNT films as anodes in Li^+ ion batteries could be attributed to the following issues: (1) SACNTs used in this work are much more flexible than normal carbon film due to their nanoscale diameter (~10 nm), resulting in highly flexible TiO_2/SACNT anodes. (2) SACNTs also function as an integrated 3-dimensioanl (3D) conductive network which greatly promotes the flow of electrons. (3) Small-size TiO_2 nanoparticles (<10 nm) have large contact areas with electrolyte and Li^+ ions, which offer a large amount of surface/interface Li storage sites without the Li-diffusion process, leading to high capacities even at very high charge/discharge rates. In sharp contrast to the well dispersed TiO_2 nanoparticles that are uniformly coated on the SACNT, the as-prepared TiO_2 are aggregated on the C−CNTs (Figure S2b and c). With these large TiO_2 aggregates, the capacities of TiO_2/C−CNT are lower than the value of TiO_2/SACNT at low current densities (Figure S2d), and with increasing the current density, the capacity of TiO_2/C−CNT decays very rapidly and becomes ~0 mA h g^{-1} when the current density exceeds 20 C (Figure S2d). We attribute this phenomenon to the long transport distance of electrons and Li^+ ions within the aggregated TiO_2. It suggests that our well dispersed TiO_2 nanoparticles on SACNT are indeed superior in the capacity and the rate performance.

In addition, with the increase of weight ratio of TiO_2, capacities of TiO_2/SACNT films still remain relatively unchanged at low charge/discharge rates (Figure S17a), i.e., the TiO_2/SACNT films with 28.7 and 46.3 wt % TiO_2 provide similar discharge capacities at 1, 5, and 10 C. Note that TiO_2/SACNT films with 46.3 wt % TiO_2 still reach a 136 mA h g^{-1} discharge capacity at 1 C even after 500 cycles, each with ~100% Coulombic efficiency (Figure S17b). The TiO_2/SACNT films with high TiO_2 weight ratios (e.g., 46.3 wt % and 60.8 wt %) exhibit both Li extraction/insertion and surface/interface storage processes at low scan rates (low current densities; Figure S18 and S19). At high scan rates (high current densities), however, the extraction/insertion of Li is much depressed due to the diffusion-limited process, causing the inner TiO_2 layers of TiO_2/SACNT films with high TiO_2 weight ratios to not contribute to the Li storage. Thus, the TiO_2/SACNT films with 46.3 wt % and 60.8 wt % TiO_2 exhibit lower capacities at high current densities, compared to that of the TiO_2/SACNT films with 28.7 wt % TiO_2.

Furthermore, from the viewpoint of practical applications, we prepared the free-standing TiO_2/SACNT films with up to 77.0 wt % TiO_2 (Figure 4a). If TiO_2/SACNT films with high weight ratio TiO_2 were fabricated simply by increasing the amount of concentrated ammonia−water or reaction time, bulk TiO_2 separated from SACNTs would appear in the reaction solution, resulting in poor capacities (e.g., TiO_2/SACNT films with 46.3 wt % TiO_2 in Figure S17a). With an improved sol−gel method, TiO_2 is dispersed uniformly on SACNTs and the thickness of the TiO_2 layer is ~160 nm (Figure 4b and c). The weight ratio of TiO_2 within TiO_2/SACNT films is measured to be 77.0 wt % by TGA analysis (Figure 4d). These TiO_2/SACNT films with ~15 mg cm^{-2} mass loading density of TiO_2 nanoparticles can be directly used as anodes for Li-ion batteries as well, without any binders, conductive agents, or current collectors. Their electrochemical performance is estimated based on the mass of TiO_2/SACNT films and is shown in Figure 4. Discharge capacities reach up to ~180, ~160, ~150, and ~105 mA h g^{-1} at 0.2, 0.5, 1, and 5 C, respectively, and the discharge capacity is still as high as ~190 mA h g^{-1} when current density returns to 0.1 C (Figure 4e). TiO_2/SACNT films also deliver 131 mA h g^{-1} discharge capacity at 1 C after 100 cycles with a ~100% Coulombic efficiency (Figure 4f), indicating their great potential in high-performance Li-ion batteries. The rate capacity of these highly loaded TiO_2/SACNT films could be possibly improved by using other synthesis methods (e.g., hydrothermal method)[43,44] that might coat a large amount of TiO_2 on SACNT more uniformly.

We further assemble TiO_2/SACNT-limited full coin cells with free-standing TiO_2/SACNT films as anodes and LMO/SACNT films as cathodes. LMO/SACNT films were prepared using an ultrasonic treatment with a mixture of commercially available LMO and scraped SACNT arrays in ethanol, followed

DOI: 10.1021/acssuschemeng.7b03671
ACS Sustainable Chem. Eng. 2018, 6, 3426−3433

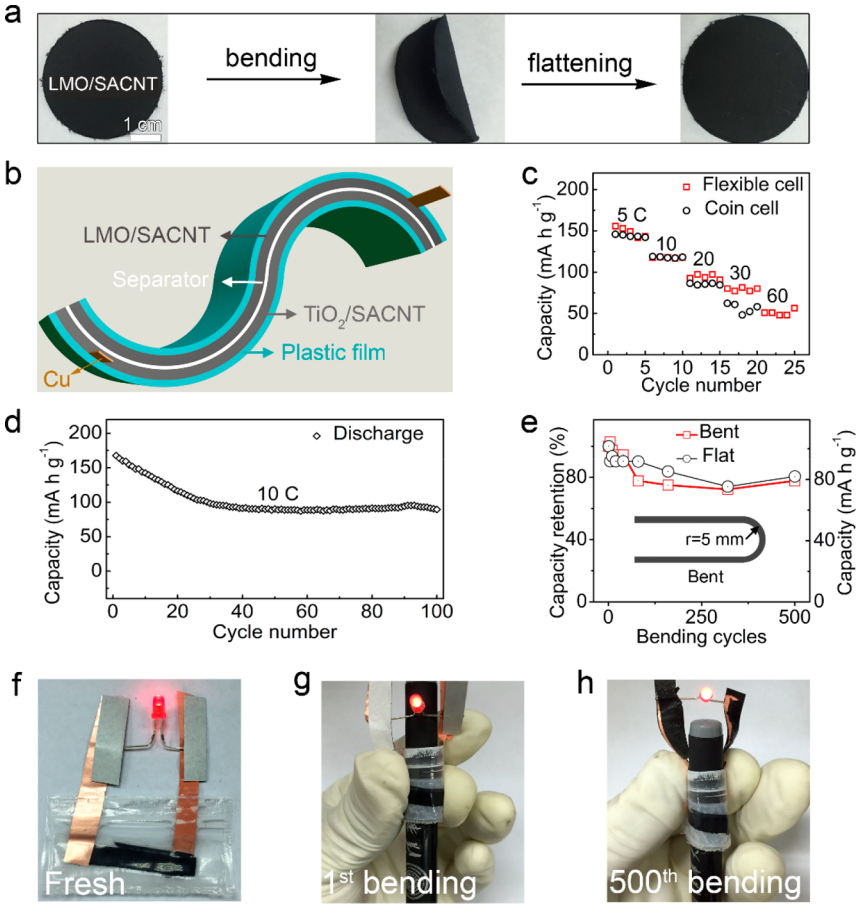

Figure 5. (a) Photos of free-standing flexible LMO/SACNT film. The flexible Li-ion cells assembled using free-standing TiO_2/CNT films as anodes and LMO/CNT films as cathodes with a cutoff voltage of 1.25−3.0 V. (b) Schematic illustration, (c) rate capacity curves, (d) cycle performance curve at 10 C over 100 cycles, (e) capacity retention curve with increasing bending cycles using a cell in the flat state as a reference, optical photographs of lighting a LED in (f) flat and (g) bent state, and (h) after bent 500 cycles.

by a vacuum filtration, a similar process to the fabrication of TiO_2/SACNT films. LMO/SACNT films are also free-standing and flexible and can be directly used as cathodes (Figure 5a and Figure S20). Figure S21a provides the galvanostatic charge/discharge curves of the full coin cells. At 1 C, a small platform at ∼1.95 V appears in the discharge curve, but it disappears due to polarization at high charge/discharge rates. As shown in Figure S21b, full cells offer high discharge capacities: ∼150, ∼145, ∼120, ∼85, and ∼60 mA h g^{-1} at 1, 5, 10, 20, and 30 C. Furthermore, these cells continue to operate a long cycle performance and still provide ∼100 mA h g^{-1} discharge capacity after 500 cycles at 10 C with Coulombic efficiency of each cycle approaching ∼100% (Figure S21c), exhibiting an excellent electrochemical performance. It is noted that the voltage of the full cells can be promoted by optimizing cathodes (e.g., $LiNi_{0.5}Mn_{1.5}O_4$). The $LiNi_{0.5}Mn_{1.5}O_4$ cathode shows a distinct voltage platform at ∼4.7 V in a half cell (Figure S22a). The platform of full cells is much increased to ∼2.6 V if the $LiNi_{0.5}Mn_{1.5}O_4$/SACNT cathode is the employed cathode (vs. $LiMn_2O_4$/SACNT cathode, only ∼1.95 V; Figure S22b).

Finally, we fabricated TiO_2/SACNT-limited flexible full cells to demonstrate their practical feasibility. There are several reports that TiO_2-based composites have been adopted as free-standing electrodes in half Li-ion batteries, such as TiO_2/graphene composites and binder-free TiO_2(B)/activated carbon fabric (ACF).[45−50] Additives (e.g., binders, current collect collectors) are usually needed to add for fabrication of the full cells.[51,52] Here, we assemble flexible full cells without binders, conductive agents, or current collectors using highly flexible TiO_2/SACNT (Figure 1g) and LMO/SACNT (Figure 5a) as anodes and cathodes, respectively, as shown in Figure 5b. Our full flexible cells demonstrate impressive capacities at various charge/discharge rates (∼150, ∼120, ∼95, ∼80, and ∼50 mA h g^{-1} at 5, 10, 20, 30, and 60 C), which are comparable to those of full coin cells (Figure 5c). Although the capacities of the full flexible cells exhibit a decay at the beginning 30 cycles, a value of ∼90 mA h g^{-1} can still be obtained at 10 C after 100 cycles (Figure 5d). The cells can be fully charged within 50 s (Figure S23) and be able to drive a LED light (working voltage at 1.8−2.0 V), regardless of being in a flat state or in a bent state (Figure 5f and g). Furthermore, we conduct bending measurements with a full cell (Figure 5e, red curve). As fast charging is much desired for flexible storage devices used in wearable electronics, we tested the flexibility of the full cells at high rates (60 C). After being bent to a curvature radius of 5 mm for 500 cycles, the full cell still has ∼80% capacity retention (a discharge capacity of ∼80 mA h g^{-1} obtained at 60 C, in contrast to an initial capacity of ∼102 mA h g^{-1}; Figure 5e, red curve). This value is almost the same as the other full cell that is never bent (Figure 5e, blue curve), indicating that the capacity decay mostly originates from other issues (such as electrolyte leakage, LMO separating from SACNT probably due to their weak interaction) rather than the bending deformation. After 500 bending cycles, the full cell can

DOI: 10.1021/acssuschemeng.7b03671
ACS Sustainable Chem. Eng. 2018, 6, 3426−3433

still light a LED without noticeable luminance decay (Figure 5h). These results suggest that our TiO_2-based flexible full cells can be a promising candidate in powering wearable electronics.

CONCLUSIONS

In conclusion, we prepare free-standing TiO_2/SACNT films using a facile *in situ* sol−gel method with SACNTs as the substrate. The flexible TiO_2/SACNT films without any binders, conductive additives, or current collectors exhibit excellent electrochemical performances when tested on half cells as anodes for Li-ion batteries. The full flexible cells are assembled as well with TiO_2/SACNT films as anodes and LMO/SACNT films as cathodes, which also demonstrate impressive electrochemical performance. The capacities of flexible cells suffer an unnoticeable decrease after 500 cycles of bending. These results suggest that our flexible films of TiO_2/SACNT composites are one of the most promising electrode materials for flexible energy storage devices. Regarding the low cost, good availability, and environmental friendliness of TiO_2, this work would be a substantial step toward the practical applications of cost-effective TiO_2-based films in flexible energy storage devices.

ASSOCIATED CONTENT

Supporting Information

The Supporting Information is available free of charge on the ACS Publications website at DOI: 10.1021/acssuschemeng.7b03671.

Photographs, SEM images, TEM images, EDX spectrum, TGA curves, XRD pattern, and electrochemical performance curves (PDF)

AUTHOR INFORMATION

Corresponding Authors

*E-mail: liuk@tsinghua.edu.cn.

*E-mail: jpwang@tsinghua.edu.cn.

ORCID

Hui Wu: 0000-0002-4284-5541

Yuegang Zhang: 0000-0003-0344-8399

Kai Liu: 0000-0002-0638-5189

Funding

This research was financially supported by the National Natural Science Foundation of China (51602173), the National Basic Research Program of China (2015CB932500), the China Postdoctoral Science Foundation (2016M591186), and the Thousand Youth Talents Program,.

Notes

The authors declare no competing financial interest.

ACKNOWLEDGMENTS

The authors acknowledge Jinghui Shi at Tianjin Jinniu Power Sources Material Co., Ltd. for providing the electrolyte, Qiang Zhang for providing commericial CNT samples, and Ke Wang for providing $LiNi_{0.5}Mn_{1.5}O_4$ powders.

REFERENCES

(1) Bao, Z.; Chen, X. Flexible and Stretchable Devices. *Adv. Mater.* **2016**, *28*, 4177−4179.

(2) Huang, S.; Zhao, C.; Pan, W.; Cui, Y.; Wu, H. Direct writing of half-meter long CNT based fiber for flexible electronics. *Nano Lett.* **2015**, *15*, 1609−1614.

(3) Dai, X.; Wu, J.; Qian, Z.; Wang, H.; Jian, J.; Cao, Y.; Rummeli, M. H.; Yi, Q.; Liu, H.; Zou, G. Ultra-smooth glassy graphene thin films for flexible transparent circuits. *Sci. Adv.* **2016**, *2*, e1601574.

(4) Oh, J. Y.; Rondeau-Gagné, S.; Chiu, Y.-C.; Chortos, A.; Lissel, F.; Wang, G.-J. N.; Schroeder, B. C.; Kurosawa, T.; Lopez, J.; Katsumata, T.; et al. Intrinsically stretchable and healable semiconducting polymer for organic transistors. *Nature* **2016**, *539*, 411−415.

(5) Zeng, Y.; Lin, Z.; Meng, Y.; Wang, Y.; Yu, M.; Lu, X.; Tong, Y. Flexible Ultrafast Aqueous Rechargeable Ni//Bi Battery Based on Highly Durable Single-Crystalline Bismuth Nanostructured Anode. *Adv. Mater.* **2016**, *28*, 9188−9195.

(6) Zhang, X.; Zhang, H.; Lin, Z.; Yu, M.; Lu, X.; Tong, Y. Recent advances and challenges of stretchable supercapacitors based on carbon materials. *Sci. China Mater.* **2016**, *59*, 475−494.

(7) Nishide, H.; Oyaizu, K. Toward flexible batteries. *Science* **2008**, *319*, 737−738.

(8) Zhou, G.; Li, F.; Cheng, H.-M. Progress in flexible lithium batteries and future prospects. *Energy Environ. Sci.* **2014**, *7*, 1307−1338.

(9) Wang, X.; Lu, X.; Liu, B.; Chen, D.; Tong, Y.; Shen, G. Flexible Energy-Storage Devices: Design Consideration and Recent Progress. *Adv. Mater.* **2014**, *26*, 4763−4782.

(10) Liu, W.; Song, M. S.; Kong, B.; Cui, Y. Flexible and Stretchable Energy Storage: Recent Advances and Future Perspectives. *Adv. Mater.* **2017**, *29*, 1603436.

(11) Zhu, K.; Sun, Y.; Wang, R.; Shan, Z.; Liu, K. Fast synthesis of uniform mesoporous titania submicrospheres with high tap densities for high-volumetric performance Li-ion batteries. *Sci. China Mater.* **2017**, *60*, 304−314.

(12) Xu, S.; Zhang, Y.; Cho, J.; Lee, J.; Huang, X.; Jia, L.; Fan, J. A.; Su, Y.; Su, J.; Zhang, H.; et al. Stretchable batteries with self-similar serpentine interconnects and integrated wireless recharging systems. *Nat. Commun.* **2013**, *4*, 1543.

(13) Wang, J.-G.; Jin, D.; Zhou, R.; Li, X.; Liu, X.-r.; Shen, C.; Xie, K.; Li, B.; Kang, F.; Wei, B. Highly Flexible Graphene/Mn_3O_4 Nanocomposite Membrane as Advanced Anodes for Li-Ion Batteries. *ACS Nano* **2016**, *10*, 6227−6234.

(14) Pushparaj, V. L.; Shaijumon, M. M.; Kumar, A.; Murugesan, S.; Ci, L.; Vajtai, R.; Linhardt, R. J.; Nalamasu, O.; Ajayan, P. M. Flexible energy storage devices based on nanocomposite paper. *Proc. Natl. Acad. Sci. U. S. A.* **2007**, *104*, 13574−13577.

(15) Noerochim, L.; Wang, J.-Z.; Chou, S.-L.; Wexler, D.; Liu, H.-K. Free-standing single-walled carbon nanotube/SnO_2 anode paper for flexible lithium-ion batteries. *Carbon* **2012**, *50*, 1289−1297.

(16) Wu, Y.; Wu, H.; Luo, S.; Wang, K.; Zhao, F.; Wei, Y.; Liu, P.; Jiang, K.; Wang, J.; Fan, S. Entrapping electrode materials within ultrathin carbon nanotube network for flexible thin film lithium ion batteries. *RSC Adv.* **2014**, *4*, 20010−20016.

(17) Chen, Z.; To, J. W.; Wang, C.; Lu, Z.; Liu, N.; Chortos, A.; Pan, L.; Wei, F.; Cui, Y.; Bao, Z. A Three-Dimensionally Interconnected Carbon Nanotube-Conducting Polymer Hydrogel Network for High-Performance Flexible Battery Electrodes. *Adv. Energy Mater.* **2014**, *4*, 1400207.

(18) Hu, L.; Wu, H.; La Mantia, F.; Yang, Y.; Cui, Y. Thin, flexible secondary Li-ion paper batteries. *ACS Nano* **2010**, *4*, 5843−5848.

(19) Li, N.; Chen, Z.; Ren, W.; Li, F.; Cheng, H.-M. Flexible graphene-based lithium ion batteries with ultrafast charge and discharge rates. *Proc. Natl. Acad. Sci. U. S. A.* **2012**, *109*, 17360−17365.

(20) Eder, D. Carbon nanotube-inorganic hybrids. *Chem. Rev.* **2010**, *110*, 1348−1385.

(21) Han, W.-Q.; Zettl, A. Coating single-walled carbon nanotubes with tin oxide. *Nano Lett.* **2003**, *3*, 681−683.

(22) Park, J. H.; Ko, J. M.; Ok Park, O. Carbon nanotube/RuO_2 nanocomposite electrodes for supercapacitors. *J. Electrochem. Soc.* **2003**, *150*, A864−A867.

(23) Ata-Ur-Rehman, A.; Ali, G.; Badshah, A.; Chung, K. Y.; Nam, K.-W.; Jawad, M.; Arshad, M.; Abbas, S. M. Superior shuttling of lithium and sodium ions in manganese-doped titania @ functionalized multiwall carbon nanotube anodes. *Nanoscale* **2017**, *9*, 9859−9871.

DOI: 10.1021/acssuschemeng.7b03671
ACS Sustainable Chem. Eng. 2018, 6, 3426−3433

(24) Cao, L.; Scheiba, F.; Roth, C.; Schweiger, F.; Cremers, C.; Stimming, U.; Fuess, H.; Chen, L.; Zhu, W.; Qiu, X. Novel Nanocomposite Pt/RuO_2· *x* H_2O/Carbon Nanotube Catalysts for Direct Methanol Fuel Cells. *Angew. Chem., Int. Ed.* **2006**, *45*, 5315−5319.
(25) Jitianu, A.; Cacciaguerra, T.; Benoit, R.; Delpeux, S.; Beguin, F.; Bonnamy, S. Synthesis and characterization of carbon nanotubes-TiO_2 nanocomposites. *Carbon* **2004**, *42*, 1147−1151.
(26) Zhang, Y.; Franklin, N. W.; Chen, R. J.; Dai, H. Metal coating on suspended carbon nanotubes and its implication to metal-tube interaction. *Chem. Phys. Lett.* **2000**, *331*, 35−41.
(27) Ayissi, S.; Charpentier, P. A.; Palotás, K. n.; Farhangi, N.; Schwarz, F.; Hofer, W. A. Preferential Adsorption of TiO_2 Nanostructures on Functionalized Single-Walled Carbon Nanotubes: A DFT Study. *J. Phys. Chem. C* **2015**, *119*, 15085−15093.
(28) Liang, Y. T.; Vijayan, B. K.; Lyandres, O.; Gray, K. A.; Hersam, M. C. Effect of dimensionality on the photocatalytic behavior of carbon-titania nanosheet composites: charge transfer at nanomaterial interfaces. *J. Phys. Chem. Lett.* **2012**, *3*, 1760−1765.
(29) Li, W.; Wang, F.; Feng, S.; Wang, J.; Sun, Z.; Li, B.; Li, Y.; Yang, J.; Elzatahry, A. A.; Xia, Y.; Zhao, D. Sol-gel design strategy for ultradispersed TiO_2 nanoparticles on graphene for high-performance lithium ion batteries. *J. Am. Chem. Soc.* **2013**, *135*, 18300−18303.
(30) Qiu, B.; Xing, M.; Zhang, J. Mesoporous TiO_2 nanocrystals grown in situ on graphene aerogels for high photocatalysis and lithium-ion batteries. *J. Am. Chem. Soc.* **2014**, *136*, 5852−5855.
(31) Guan, B. Y.; Yu, L.; Li, J.; Lou, X. W. D. A universal cooperative assembly-directed method for coating of mesoporous TiO_2 nanoshells with enhanced lithium storage properties. *Sci. Adv.* **2016**, *2*, e1501554.
(32) Eftekhari, A. Lithium-Ion Batteries with High Rate Capabilities. *ACS Sustainable Chem. Eng.* **2017**, *5*, 2799−2816.
(33) Liu, H.; Li, W.; Shen, D.; Zhao, D.; Wang, G. Graphitic carbon conformal coating of mesoporous TiO_2 hollow spheres for high-performance lithium ion battery anodes. *J. Am. Chem. Soc.* **2015**, *137*, 13161−13166.
(34) Liu, K.; Jiang, K.; Wei, Y.; Ge, S.; Liu, P.; Fan, S. Controlled Termination of the Growth of Vertically Aligned Carbon Nanotube Arrays. *Adv. Mater.* **2007**, *19*, 975−978.
(35) Liu, K.; Sun, Y.; Chen, L.; Feng, C.; Feng, X.; Jiang, K.; Zhao, Y.; Fan, S. Controlled growth of super-aligned carbon nanotube arrays for spinning continuous unidirectional sheets with tunable physical properties. *Nano Lett.* **2008**, *8*, 700−705.
(36) Jiang, K.; Wang, J.; Li, Q.; Liu, L.; Liu, C.; Fan, S. Superaligned carbon nanotube arrays, films, and yarns: a road to applications. *Adv. Mater.* **2011**, *23*, 1154−1161.
(37) Wang, S.; Pan, L.; Song, J.-J.; Mi, W.; Zou, J.-J.; Wang, L.; Zhang, X. Titanium-defected undoped anatase TiO_2 with p-type conductivity, room-temperature ferromagnetism, and remarkable photocatalytic performance. *J. Am. Chem. Soc.* **2015**, *137*, 2975−2983.
(38) Zhu, K.; Liu, X.; Du, J.; Tian, J.; Wang, Y.; Liu, S.; Shan, Z. In situ synthesis of mesoporous single-grain layer anatase TiO_2 nanosheets without additives via a mild and simple process for a long-term Li-ion battery. *J. Mater. Chem. A* **2015**, *3*, 6455−6463.
(39) Wang, J.; Polleux, J.; Lim, J.; Dunn, B. Pseudocapacitive contributions to electrochemical energy storage in TiO_2 (anatase) nanoparticles. *J. Phys. Chem. C* **2007**, *111*, 14925−14931.
(40) Yang, S.; Feng, X.; Müllen, K. Sandwich-Like, Graphene-Based Titania Nanosheets with High Surface Area for Fast Lithium Storage. *Adv. Mater.* **2011**, *23*, 3575−3579.
(41) Zhou, T.; Zheng, Y.; Gao, H.; Min, S.; Li, S.; Liu, H. K.; Guo, Z. Surface Engineering and Design Strategy for Surface-Amorphized TiO_2@ Graphene Hybrids for High Power Li-Ion Battery Electrodes. *Adv. Sci.* **2015**, *2*, 1500027.
(42) Wang, D.; Choi, D.; Li, J.; Yang, Z.; Nie, Z.; Kou, R.; Hu, D.; Wang, C.; Saraf, L. V.; Zhang, J.; Aksay, I. A.; Liu, J. Self-assembled TiO_2-graphene hybrid nanostructures for enhanced Li-ion insertion. *ACS Nano* **2009**, *3*, 907−914.
(43) Balogun, M.-S.; Zhu, Y.; Qiu, W.; Luo, Y.; Huang, Y.; Liang, C.; Lu, X.; Tong, Y. Chemically lithiated TiO_2 heterostructured nanosheet anode with excellent rate capability and long cycle life for high-performance lithium-ion batteries. *ACS Appl. Mater. Interfaces* **2015**, *7*, 25991−26003.
(44) Lu, X.; Wang, G.; Zhai, T.; Yu, M.; Gan, J.; Tong, Y.; Li, Y. Hydrogenated TiO_2 nanotube arrays for supercapacitors. *Nano Lett.* **2012**, *12* (3), 1690−1696.
(45) Zhao, B.; Cai, R.; Jiang, S.; Sha, Y.; Shao, Z. Highly flexible self-standing film electrode composed of mesoporous rutile TiO_2/C nanofibers for lithium-ion batteries. *Electrochim. Acta* **2012**, *85*, 636−643.
(46) Hu, T.; Sun, X.; Sun, H.; Yu, M.; Lu, F.; Liu, C.; Lian, J. Flexible free-standing graphene-TiO_2 hybrid paper for use as lithium ion battery anode materials. *Carbon* **2013**, *51*, 322−326.
(47) Wei, D.; Andrew, P.; Yang, H.; Jiang, Y.; Li, F.; Shan, C.; Ruan, W.; Han, D.; Niu, L.; Bower, C.; et al. Flexible solid state lithium batteries based on graphene inks. *J. Mater. Chem.* **2011**, *21*, 9762−9767.
(48) Li, N.; Zhou, G.; Fang, R.; Li, F.; Cheng, H.-M. TiO_2/graphene sandwich paper as an anisotropic electrode for high rate lithium ion batteries. *Nanoscale* **2013**, *5*, 7780−7784.
(49) Liu, S.; Wang, Z.; Yu, C.; Wu, H. B.; Wang, G.; Dong, Q.; Qiu, J.; Eychmüller, A.; David Lou, X. W. A flexible TiO_2 (B)-based battery electrode with superior power rate and ultralong cycle life. *Adv. Mater.* **2013**, *25*, 3462−3467.
(50) Zhang, P.; Qiu, J.; Zheng, Z.; Liu, G.; Ling, M.; Martens, W.; Wang, H.; Zhao, H.; Zhang, S. Free-standing and bendable carbon nanotubes/TiO_2 nanofibres composite electrodes for flexible lithium ion batteries. *Electrochim. Acta* **2013**, *104*, 41−47.
(51) Wang, X. H.; Guan, C.; Sun, L. M.; Susantyoko, R. A.; Fan, H. J.; Zhang, Q. Highly stable and flexible Li-ion battery anodes based on TiO_2 coated 3D carbon nanostructures. *J. Mater. Chem. A* **2015**, *3*, 15394−15398.
(52) Huang, H.-B.; Yang, Y.; Chen, L.-H.; Wang, Y.; Huang, S.-Z.; Tao, J.-W.; Ma, X.-T.; Hasan, T.; Li, Y.; Xu, Y.; Su, B.-L. Hierarchical TiO_2/C nanocomposite monoliths with a robust scaffolding architecture, mesopore-macropore network and TiO_2-C heterostructure for high-performance lithium ion batteries. *Nanoscale* **2016**, *8*, 10928−10937.

DOI: 10.1021/acssuschemeng.7b03671
ACS Sustainable Chem. Eng. 2018, 6, 3426−3433